J. Fluid Mech. (2001), *vol.* 437, *pp.* 203–228. Printed in the United Kingdom

Hydrodynamical similarities between bubble column and bubbly pipe flow

By ROBERT F. MUDDE† AND TAKAYUKI SAITO‡

National Institute For Resources and Environment, 16-3 Onogawa, Tsukuba, Ibaraki 305-8569, Japan

(Received 18 May 2000 and in revised form 10 October 2000)

The hydrodynamical similarities between the bubbly flow in a bubble column and in a pipe with vertical upward liquid flow are investigated. The system concerns air/water bubbly flow in a vertical cylinder of 14.9 cm inner diameter. Measurements of the radial distribution of the liquid velocity, gas fraction and the bubble velocity and size are performed using laser Doppler anemometry for the liquid velocity and a four-point optical fibre probe for the gas fraction, bubble velocity and size. The averaged gas fraction was 5.2% for the bubble column (with a superficial liquid velocity of zero) and 5.5% for the bubbly pipe flow at a superficial liquid velocity of $0.175\,\mathrm{m\,s^{-1}}$. From a hydrodynamical point of view, the two modes of operation are very similar. It is found that in many respects the bubbly pipe flow is the superposition of the flow in the bubble column mode and single-phase flow at the same superficial liquid velocity.

The radial gas fraction profiles are the same and the velocity profiles differ only by a constant offset: the superficial liquid velocity. This means that the well-known large-scale liquid circulation (in a time-averaged sense) of the bubble column is also present in the bubbly pipe flow. For the turbulence intensities it is found that the bubbly pipe flow is like the superposition of the bubble column and the single-phase flow at the superficial liquid velocity of the pipe flow, the former being at least an order of magnitude higher than the latter. The large vortical structures that have been found in the bubble columns are also present in the bubbly pipe flow case, partly explaining the much higher 'turbulence' levels observed.

1. Introduction

Bubbly flows are found in numerous industrial applications. Two typical reactors used are: (i) the bubble column, in which the liquid phase is 'stagnant', i.e. no net liquid flow through a cross-section perpendicular to the column axis is present; and (ii) the air lift reactor in which the liquid phase circulates through the reactor under the action of gravity (see figure 1 for a schematic representation). Both types of reactors are popular due to their simple construction, good mixing properties and rather low shear rates. Applications are found in the chemical industry, in waste water treatment and in biotechnology (see e.g. Deckwer 1992). Many papers can be found that deal with these reactors. However, the number of papers on the local hydrodynamics is

† Corresponding author, permanent address: Kramers Laboratorium voor Fysische Technologie, Delft University of Technology, Pr. Bernhardl. 6, 2628BW Delft, The Netherlands.

‡ Also at: Department of Mechanical Engineering, Faculty of Engineering, Shizuoka University, 3-5-1, Johoku, Hamamatsu 432-8561, Japan.

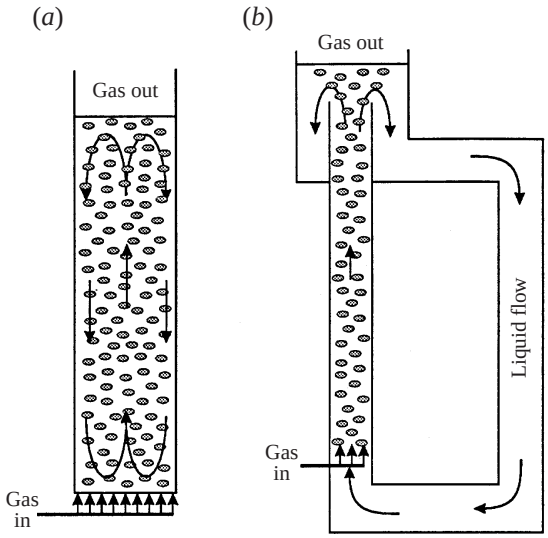

FIGURE 1. Schematic representation of the bubble column (*a*) and the air lift reactor (*b*). The arrows indicate the time-averaged liquid flow.

rather limited, especially when dealing with both the liquid flow field and the bubble-phase characteristics. Regarding the structure of the turbulence, there are even fewer reports. During the last decade, when computational fluid dynamics (CFD) became a promising tool for designing bubble reactors, the details of the bubbly flow received more attention. Nevertheless, modelling of the flow is still far from straightforward. In the case of the bubble column the overall behaviour can be assessed to some extend via the theoretical work of e.g. Ueyama & Miyauchi (1979), Geary & Rice (1992) or Gharat & Joshi (1992). For the air lift one can use a one-dimensional description based on a mechanical energy balance and a drift flux model to couple the gas and liquid phase (see e.g. Chisti, Halrd & Moo-Young 1988, Young, Carbonell & Ollis 1991). However, CFD approaches offer a much greater potential for designing and fine tuning of the bubble reactors. In recent work some CFD simulations on bubble columns and air lifts can be found, see e.g. Grevskott *et al.* (1996), Cockx *et al.* (1997), Sanyal *et al.* (1999), Bauer & Eigenberger (1999) and Cockx *et al.* (1999).

Two-phase flow in a bubble reactor is a complicated phenomenon. For bubble columns, the liquid exhibits a large-scale circulation in a time-averaged sense: upward flow of the liquid in the centre of the column, downward flow in the wall region (see figure 1). The first reliable data on this large-scale circulation date back to the work of Hills (1974). Based on the findings of Hills, Ueyama & Miyauchi (1979) modelled the flow field using a one-dimensional balance equation for the momentum of the mixture. They used a prescribed radial gas fraction profile as input. In this way they could obtain reasonable agreement with the experimental data. In 1984 Franz *et al.* (1984) reported on the motion of so-called vortical structures that were present in the flow: eddy-like structures that move through the bubbly mixtures with sizes on the order of the column diameter. The vortical structures have been extensively studied in the group of L.-S. Fan (see e.g. Chen, Reese & Fan 1994; Lin *et al.* 1996; Mudde *et al.* 1997*b*) as well as by Groen, Mudde & Van Den Akker (1995), Groen *et al.* (1996), Mudde, Groen & Van Den Akker (1997*a*) and by Devanathan (1991). In flat (two-dimensional) columns they move in a very periodic way from the free

surface downwards; in cylindrical columns their motion is much more chaotic. They appear at a given location at a frequency less than 0.1 Hz. As a consequence of these vortical structures, the standard deviation of e.g. the axial liquid velocity is easily as large as or larger than the time-averaged axial velocity. Obviously, they contribute to the turbulence intensity defined as the standard deviation over the (local) time-averaged liquid velocity. This intensity is large, especially around the cross-over from time-averaged upward to downward liquid flow.

The vortical structures are also important when dealing with the back mixing in the column. They are strong enough to not only slow down locally the gas bubbles but even drag them downwards. The large-scale structures are a consequence of gravity that acts on non-uniform distributions of the bubbles. The instability generated gives rise to the occurrence of the vortical structures. Excellent examples can be found in the work on two-dimensional columns, see e.g. Lin *et al.* (1996), Mudde *et al.* (1997*b*). Experiments with a radioactive liquid flow tracer using the CARPT facility (Yang, Devanathan & Duduković 1993) show the same features, but then in a Lagrangian way.

Air lift reactors are supposed to be in a much less chaotic state. They are in a first approximation regarded as plug flow reactors, i.e. the back mixing of the bubbles and of the liquid is small. However, several researchers have pointed out the possibility of circulatory motion in the riser part, see e.g. Mercer (1990) who reported from visual observation: "Upward motion of bubbles was observed predominantly in the center of the riser while downward motion was observed along the glass walls. This downward motion was frequently disrupted as the pattern shifted and the flow markers were drawn repeatedly into the central area of the column". From this quote it is easy to envision great similarity between the (time-dependent) hydrodynamics in an air lift reactor and a bubble column. Not many papers dealing with local phenomena in air lift reactors have appeared; most of the work deals with a more global description of the flow phenomena. A good example of experiments on local phenomena is Young *et al.* (1991). In their work the gas fraction profiles are obtained using gamma densitometry and a resistivity probe. The liquid velocity is measured using a hot-wire. As the work is focussed on air lift reactors, no measurements were reported for the bubble column mode (i.e. zero net liquid flow rate). From Young *et al.* (1991) it is clear that the radial profile of the axial liquid velocity in the riser is much less flat than for the familiar single phase turbulent flows. The velocity in the centre is much higher than close to the wall. Furthermore, at not too low gas flow rates, the gas fraction in the centre is higher than in the wall region. A fit of their gas fraction data showed that the gas fraction profile had a power-law-like behaviour, the exponent ranging from 1.6 to 2.2. Recently, Ohnuki & Akimoto (2000) reported experimental data on the distribution of the gas fraction in vertical pipes of larger diameters. They showed that at a given superficial gas velocity the transition from wall peaking to core peaking of the gas fraction occurs at lower superficial liquid velocity if the pipe diameter is increased. Based on their data, the gas fraction in the present experiments should be core peaking for both the bubble column and the air lift mode.

The aim of this contribution is to investigate the local flow phenomena in both reactor types and study the similarities and differences between a completely gravity-driven flow (the bubble column) and a bubbly flow that is induced by a pressure difference (i.e. via a pump) as well as by gravity. Therefore, a setup has been built in which the bubbly flow can be either in the bubble column mode, i.e. no throughput of liquid, or in the air lift mode (namely bubbly pipe flow), i.e. a net upward liquid

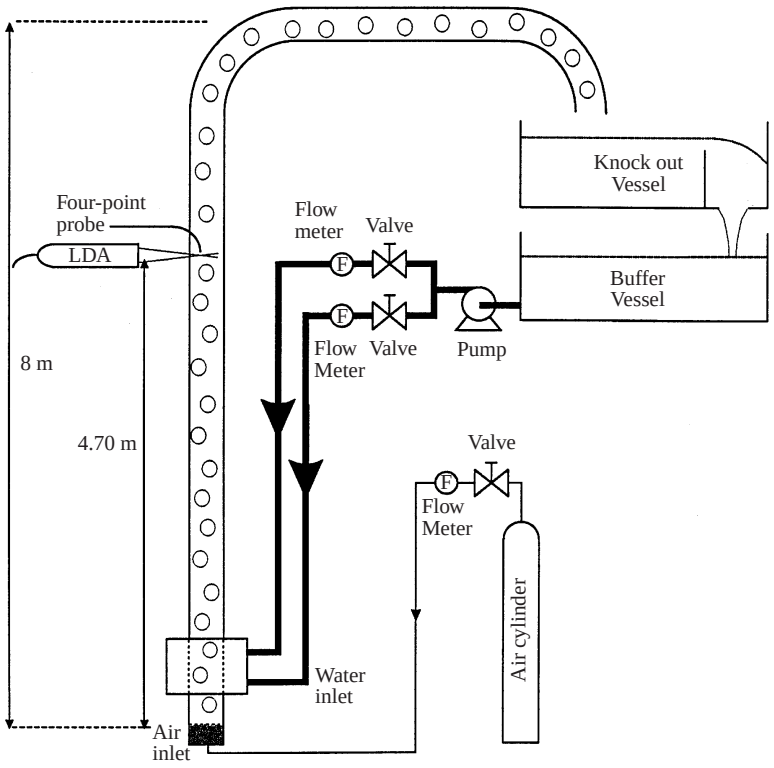

FIGURE 2. Experimental setup.

flow is induced by means of a pump. The structure of the turbulent bubbly flow has been investigated experimentally in a long vertical pipe. The experiments aim at comparing the bubbly flow in the case of a bubble column with that of an air lift at the same averaged gas fraction in a well-developed region of the flow (i.e. high above the gas and liquid inlet). The data are collected using laser Doppler anemometry (LDA) for the liquid velocity and a four-point optical fibre probe for the gas fraction and bubble size and velocity. The time-averaged profiles of the liquid velocity and the bubble velocity are studied, and the local turbulence is compared by evaluating the velocity fluctuations of the liquid. For reference, some properties of single-phase flow at the same superficial velocity (giving a Reynolds number of 2.6×10^4) as for the experiments of the air lift mode are given.

2. Setup

2.1. *Vertical loop*

The experiments were performed in a vertical pipe with an inner diameter of 14.9 cm. This pipe is part of a flow loop (see figure 2). The height of the pipe is 8.0 m; the experiments are performed at a height of 4.70 m above the gas distributor. The water that flows out of the riser part is first fed to a knockout vessel (volume 3 m^3). Via a weir the water flows into a buffer vessel (volume 3 m^3). A pump circulates the water via two flow lines (inner diameter 50 mm) back to the bottom part of the riser section, where it joins the bubbly flow via a special water inlet section that promotes quick mixing. The water flow can be controlled by two valves and is

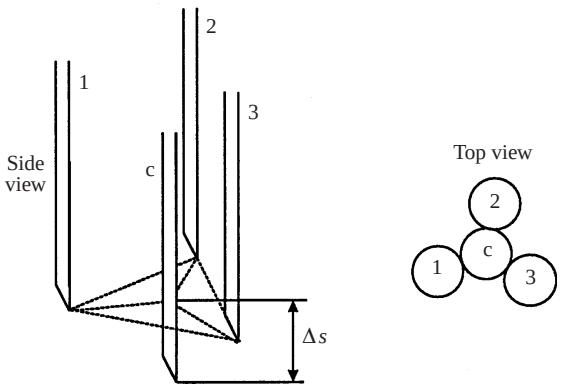

FIGURE 3. Schematic representation of the optical four-point probe.

measured by two electro-magnetic flow meters (type ADMAG-AE-50A, Yokogawa Electric Corporation, range 0–5 m s^{-1}, accuracy 0.5% of indicated value). Air from a cylinder is introduced into the riser at the bottom via a porous medium with a bed of glass beads of 1.5 mm diameter. Visual inspection shows that the majority of the bubbles generated are ellipsoidal in shape with a long, horizontal axis of about 4.5 mm and a short, vertical axis of 2.5 mm. The air flow is measured with a mass flow meter (MASFLO-OVAL, range 0–100N l min^{-1}, accuracy 1% of full scale). For all experiments plain tap water was used. The LDA experiments are carried out using a 4W Spectra-Physics Ar^+ laser and TSI LDA equipment (colorburst TRCF-2, colorlink TRCF-2, IFA755 automatic burst correlator and TSI-FIND software). The frequency shift is 500 kHz, and the total power of the laser is 1.2 W. The lens of the LDA probe has a focal distance of 250 mm, and the beam spacing is 5 cm giving a measuring volume with a length and width of approximately 1.3 mm and 0.1 mm, respectively.

The seeding particles used are of polystyrene with a diameter of (15 ± 5) μm and a density of 1.1×10^3 kg m^{-3}. The laser beams enter the bubbly mixture via the (Perspex) pipe. Consequently, the beam pair for the vertical velocity component is refracted to a different radial position than the pair for the tangential component. The difference between the two is larger when measuring deeper in the column. Thus, with the present setup no radial profile of the Reynolds shear stress (i.e. its axial-tangential component) can be obtained.

2.2. *Optical probe*

For measuring the gas fraction distribution as well as the radial distribution of the bubble size and velocity an in-house made optical glass fibre probe has been utilized (Frijlink 1987; Cartellier 1992). The probe consists of four fibres (Polymethyl Meta Acrylate), each with a diameter of 0.2 mm. Three of the tips of the probe are of the same length and form an equilateral triangle. The fourth, central one is positioned through the centre of gravity of this triangle and is about 1.5 mm longer than the others (see figure 3). The radial distance from the central probe to each of the others is about 0.5 mm.

The tip of each of the fibres is cut to an angle of 30° with the fibre axis; light is send into each fibre. If water is present at the tip most of the light enters the water in view of the relatively small difference in refractive index between the fibre material and water. If, on the other hand, an air bubble is pierced by a tip most of the light is

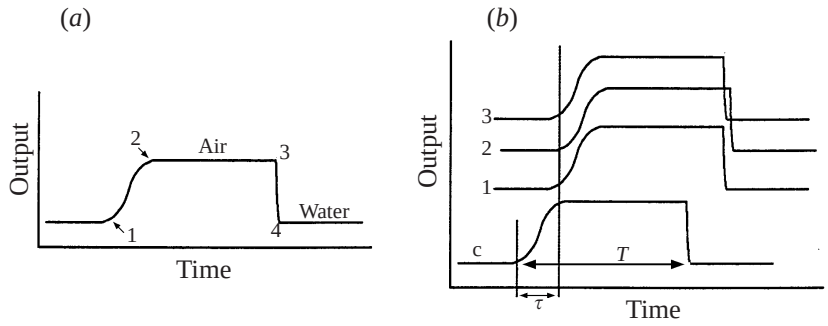

FIGURE 4. (*a*) Response of a probe tip to the passage of a bubble; (*b*) response of the four points of the probe to the passage of a bubble.

reflected back into the probe and detected at the other side using a photo multiplier (one for each fibre, type R212, Hamamatsu Photonic Co., Ltd.). The output of each of the tips is sampled at a sampling frequency of 20 kHz or 40 kHz, depending on the bubble velocities expected. This is a compromise between accuracy on the one hand and number of samples that can be stored on the other hand. The typical response of the probe when a bubble passes is illustrated in figure 4.

As can be seen from figure 4(*a*), when a bubble hits a fibre tip, the output of that fibre rises as more of the tip surface will reflect light. When the tip is completely inside the bubble the output is constant. As the tip touches the bubble–water surface again, the response is much faster as the surface tension will cause the bubble surface to quickly 'shoot upwards' along the fibre. If a bubble hits the four-point probe with its velocity vector parallel to the fibres, the response of the fibres is like in figure 4(*b*). The central one (*c*), which is a little longer will react first, followed by the other three which respond almost simultaneously. From the central tip the local gas fraction, defined as the time this tip is in air with respect to the total measuring time, is obtained. From careful analysis of the four outputs simultaneously, the bubble velocity component parallel to the fibres and the bubble diameter in this direction can be obtained. This will be explained in more detail in the next section.

The probe is fitted into a capillary, that is bent at the end at an angle of 90°. The probe is inserted into the column wall, such that it can be traversed over the column diameter, parallel to the traversing direction of the LDA-measuring volume. The end of the actual sensor is aligned vertically and the tips are facing downwards.

3. Signal analysis

3.1. *Optical probe*

The optical probe provides four time series $s_i(t_j)$, with $i = \mathrm{c}, 1, 2, 3$. The gas fraction is obtained from s_c. First this time series is made binary via an appropriate threshold (th_α) which is set at 15% of the difference between the output value of tip c in air and that in water:

$$b_c(t_j) = \begin{cases} 1 & \text{if } s_c(t_j) > th_\alpha \\ 0 & \text{otherwise.} \end{cases} \tag{1}$$

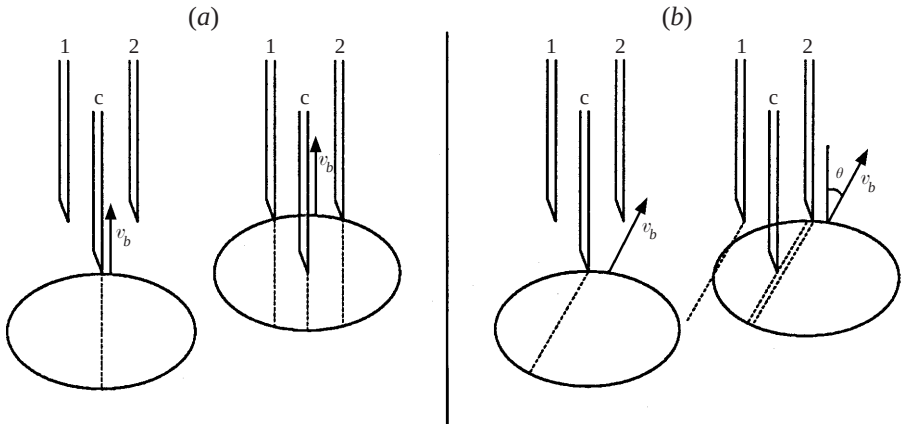

FIGURE 5. Bubble pierced by probe: (*a*) vertical bubble rise, hit symmetrically; (*b*) bubble rises under an angle, θ, with the probe: no simultaneous response from tip 1 and 2. For clarity tip 3 is not drawn.

Next the (local) gas fraction is obtained as

$$\alpha = \frac{\sum_{j=1}^{N} b_c(t_j)\Delta t_s}{N\Delta t_s} \tag{2}$$

with N the total number of samples and Δt_s the sample time.

The threshold should not be too high as this would cause bubbles that touch the tip rather than being pierced, to be filtered out thus underestimating the gas fraction. Obviously, it cannot be too close to 0 as then unwanted noise would cause an overestimate of the gas fraction. The 15% criterion is an optimum value for the tip used. Variation of the threshold shows that below a value of 10% the measured gas fraction increases relatively steeply with the threshold value. Above a threshold value of 10% the sensitivity to the choice of the threshold value is $\mathrm{d}\alpha/\mathrm{d}th_\alpha = -0.01$ (with both α and th_α represented as a fraction between 0 and 1).

Determination of the bubble velocity and bubble size is more complicated. In principle, the direction of the bubble motion is unknown. Furthermore, the bubble shape may vary, e.g. with the bubble size. For the analysis it is assumed that the bubbles have an ellipsoidal or a spherical cap shape. Visual inspection of the bubbly flow showed that the majority of the bubbles have an ellipsoidal shape with a horizontal diameter of some 4.5 mm and a vertical one of about 2.5 mm. From this and the probe dimensions the following algorithm (Frijlink 1987) is used to determine the vertical component of the bubble velocity as well as the bubble vertical diameter. A bubble that moves vertically upwards and hits the probe will cause a response on the central tip first and a little later on the other three (see figure 4*b*). By requiring that the response of tips 1, 2, 3 is (almost) simultaneous it is ensured that (i) the bubble moves vertically upwards and (ii) the probe measures the vertical bubble diameter, i.e. the chordal trajectory of the central tip through the bubble is along the vertical diameter of the bubble (see e.g. Frijlink 1987). If the bubble is hit too much to the side, the chordal trajectory of the central tip will be different from the vertical bubble diameter (see figure 5). However, in that case the response of the three tips 1, 2, 3 will not be simultaneous due to the curvature of the bubble surface. Once the time difference between the response of the tips 1, 2, 3 and that of tip c is known (i.e. the

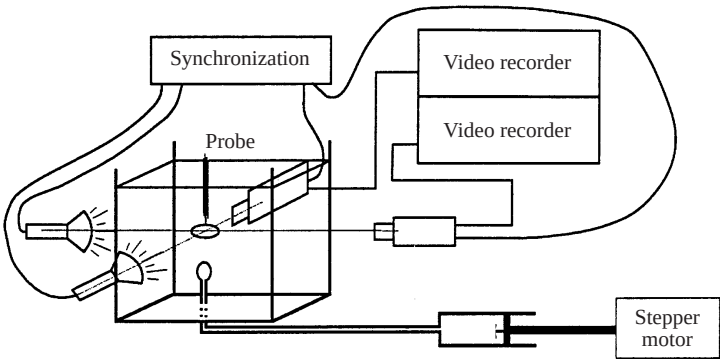

FIGURE 6. Setup for calibration of optical probe.

rise time), the velocity of the bubble follows as the ratio of the known difference in length, Δs, of the central tip and the others and the rise time. The vertical diameter is then equal to the product of the vertical velocity and the time the central tip is inside the bubble. A more detailed explanation is given in the next section.

3.2. *Probe calibration*

A careful calibration is needed to find an appropriate value for the tolerance, δt, between the simultaneous reaction of the tips 1, 2, 3. Furthermore, a second threshold value is needed at which the rise of the output signal is marked as the start of the response of a tip to the bubble piercing. For the calibration a special experiment was set up. A bubble train is generated via a capillary that is placed at the bottom of a cubical container (30 cm $\times$ 30 cm $\times$ 30 cm) filled with tap water. Air is forced through the capillary at a constant rate by pushing the piston of a large hypodermic syringe inwards using a stepper motor (see figure 6). In this way bubbles of the desired size (volume equivalent diameter about 3 mm) can be generated at a well-defined and controllable rate. The optical probe is placed several centimetres above the capillary at such a position that the bubbles hit the probe frequently (i.e. the wobbling has not deviated them too much from a vertical trajectory) and at the same time the bubble shape is in equilibrium. The bubbles hitting the probe are filmed at a frame rate of 500 Hz using two digital camera that view the bubbles at perpendicular angles. Light from two stroboscopes is used. The two cameras and the two stroboscopes are synchronized. The field of view of the cameras is 2.04 cm $\times$ 1.53 cm (horizontal by vertical size) with a resolution of 0.0319 mm/px.

From the images it is found that the vertical velocity of the bubbles is 30.5 cm s^{-1} and the vertical diameter is 2.04 mm (the horizontal size is 5.1 mm). An example of some of the images is shown in figure 7. Notice that the shape oscillations of the rising bubble can be seen clearly.

From the video images the difference, Δs, between the length of the central tip and the other three is also found: $\Delta s = 1.63$ mm. This value is used for the calculation of the bubble velocity and size. Finally, it is remarked that from the video images it was clear that the velocity of the bubble was unchanged when the bubble was pierced by the probe. This is illustrated in figure 8.

A series of 184 bubbles hitting the probe (bubble frequency 4 Hz) was recorded by the optical probe using a sampling frequency of 20 kHz. The velocity and size of the bubbles is calculated using various values for the tolerance and for the threshold that is used to decide when a bubble actually hits a tip. First, the signal of the central tip

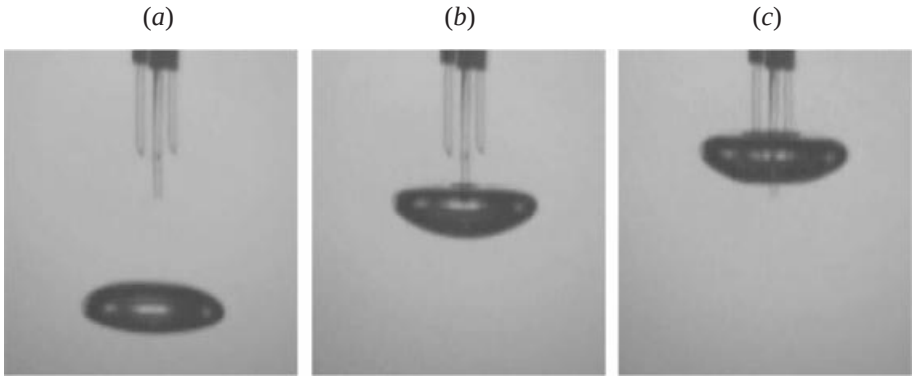

FIGURE 7. Images of a moving bubble: (*a*) bubble approaching the probe; (*b*) bubble pierced by central tip; (*c*) tips 1, 2, 3 inside bubble, central tip has left the bubble.

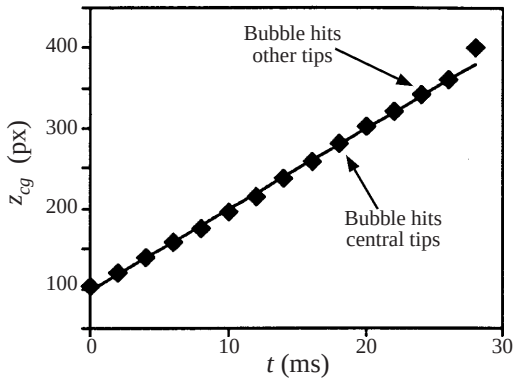

FIGURE 8. Time-trace of the vertical component of the centre of gravity of a bubble that at $t = 18$ ms hits the central tip of the probe.

is used to mark the start of a bubble. Next, from this time a search for the bubble hitting the other three probes is made. Once all three are found, the time differences, τ_{ic}, are calculated and the search is started from the next bubble that hits the central tip. The definition of τ_{ic} is as follows:

$$\left.\begin{array}{ll} \text{if } s_c(t_s) > th_v & \text{bubble hits central tip at time } t_s, \\ \text{if } s_i(t_k) > th_v & \text{bubble hits tip } i \text{ at time } t_k, \\ \tau_{ic} = t_k - t_s. & \end{array}\right\} \tag{3}$$

The next step is evaluating whether or not these three time differences do coincide within a given tolerance, δt:

$$\left.\begin{array}{ll} \tau = \frac{1}{3}\sum_{i=1}^{3} \tau_{ic} & \\ \text{if } \left|\frac{\tau_{ic}-\tau}{\tau}\right| < \delta t \ \forall i & \text{then valid bubble detection} \\ & \text{otherwise reject and reset.} \end{array}\right\} \tag{4}$$

If the absolute values of the relative time differences are all smaller than δt the

bubble is validated and the velocity, v_b, follows as

$$v_b = \frac{\Delta s}{\tau}. \tag{5}$$

Subsequently, the point at which the central tip leaves the bubble is located. From the time, T, that the central tip is inside the bubble, the vertical bubble size, d_b, is calculated:

$$\left.\begin{array}{l} \text{if} \quad s_c(t_e) < th_v \text{ central tip leaves bubble,} \\ \quad T = t_e - t_c, \\ \quad d_b = v_b T. \end{array}\right\} \tag{6}$$

The best agreement with the measured velocity and the velocity from the camera is obtained when using for the tolerance 8% of the mean time difference and for the threshold 60% of the difference between the output of a tip in air and in water. With these settings 183 out of the 184 bubbles could be used, resulting in a velocity of $31.0 \pm 0.6\,\mathrm{cm\,s^{-1}}$ and a vertical size of $1.53 \pm 0.05\,\mathrm{mm}$. The velocity is in excellent agreement with the video images; the size of the bubbles is underestimated. This is partly caused by the relatively high value of the second threshold. If this one is lowered to 20% the vertical size measured becomes $1.73 \pm 0.06\,\mathrm{mm}$. At this threshold value, the bubble velocity is $32.8 \pm 0.6\,\mathrm{cm\,s^{-1}}$. In the experiments on the bubbly flow the threshold of 60% is used as accurate determination of the velocity is more important than the bubble size. The velocity measured by the probe is rather insensitive to the exact values of the tolerance and threshold, the diameter, however, is. Note that for these bubbles the uncertainty in the measured velocity due to the finite sampling rate is about 1%. In the experiments with the pump switched on, the sampling frequency is increased to 40 kHz in view of the larger velocities.

In principle, a correction should be made in the procedure outlined above that takes into account the curvature of the bubble surface. However, as the bubbles are rather flat (horizontal to vertical size ratio about 2) no correction has been applied. A detailed analysis about this can be found in e.g. Frijlink (1987). It should be noted that the use of the four-point probe introduces a biasing in the bubble velocity data as only almost strictly vertical rising bubbles will be accepted by the analysis.

Accuracy

In the experiments on the bubbly flows, a tolerance of 20% has been used as otherwise the number of bubbles accepted by the tolerance would be rather low. The inaccuracy of the bubble velocity and size is determined by various factors. The most important ones are: the angle, θ, that the bubble velocity vector makes with the probe (i.e. the vertical in the present experiments) and the position (with respect to the centre of gravity of the bubble) at which the bubble hits the probe. To investigate the influence of the choice for the tolerance, δt, on the accuracy of the calculated velocity and size, a Monte Carlo simulation was performed in which 100 000 bubbles hit the probe. In this simulation, the bubbles were ellipsoidal with a horizontal axis of 4.5 mm and a vertical one of 2.5 mm. The bubble velocity was $25\,\mathrm{cm\,s^{-1}}$; its angle, θ, with respect to the vertical varied between 0 and $\pi/2$. The probability density function of θ was taken as $\cos(\theta)$. The radial distance, r, from the central tip of the probe to the vertical symmetry axis of the bubbles at the moment of the hit had a probability density function that varied linearly with r. In the simulations the velocity as well as the bubble size are underestimated. The error made is an increasing function of the angle the bubble velocity vector makes with the vertical. It is rather insensitive to the value

of the tolerance, δt. For the conditions of the calibration experiments (tolerance 8%, $\theta \leqslant 20^\circ$) the mean velocity from the Monte Carlo simulations is $24.2\,\mathrm{cm\,s^{-1}}$ with a standard deviation of $0.6\,\mathrm{cm\,s^{-1}}$. The mean bubble size from these simulations is 2.33 mm with a standard deviation of 0.08 mm. For the settings that mimic the real experiment the tolerance was set at 20% and θ could vary from 0 to $\pi/2$. Now, according to the simulations, the mean velocity is $(22.4 \pm 2.4)\,\mathrm{cm\,s^{-1}}$. The bubble size is found to be: (2.16 ± 0.23) mm. Reducing the maximum value of θ to $\pi/4$ hardly influences these numbers.

Finally, note that in the analysis of most data series from the real experiments (at a given flow condition and measuring position) a few bubbles with a diameter of 1 mm or less were found. These have been removed as bubbles of this size would be almost spherical and it is well known (see e.g. Frijlink 1987) that no reliable information on these can be obtained with the four-point probe in view of the probe dimensions.

3.3. *LDA*

Consider a LDA time series of the vertical liquid velocity $\{v'(t_i)\}$. The series have a length ranging from 400 to 1000 s. The number of data points per series ranges from some 70 k (in the column centre) to about 400 k (close to the wall). The averaged data rate is 100–300 Hz. Due to the nature of LDA, the sampling is taken at random times $\{t_i\}$. Furthermore, in the data spurious samples are present due to e.g. multiple scattering of the laser light. Therefore, the set is filtered: first the ensemble average, $\overline{v'}$, and the standard deviation, σ', of the series are calculated:

$$\overline{v'} = \frac{1}{N}\sum_{i=1}^{N} v'(t_i), \tag{7}$$

$$\sigma' = \left[\frac{1}{N}\sum_{i=1}^{N}\left(v'(t_i) - \overline{v'}\right)^2\right]^{1/2}. \tag{8}$$

Next, data points that are outside the band $(\overline{v'} \pm 3\sigma')$ are removed from the set. Subsequently, for the filtered set $\{v_i\}$ the mean, $\langle v\rangle$, and standard deviation, σ, are calculated. This is the same procedure as used by Mudde & Van Den Akker (1999).

The time-series analysis of the LDA-velocity data is complicated due to the presence of the bubbles in the flow. The distribution of the time between two consecutive data points becomes wider than in the single-phase case: bubbles will block at irregular times one of the laser beams (see Mudde, Groen & Van Den Akker 1998; Mudde *et al.* 1997*a*). The time-between-data distribution no longer follows the well-known Poisson distribution. An example of a time series of the axial velocity component and its corresponding time-between-data distribution is given in figure 9.

As can be seen from the figure, relatively large gaps in the data are present. In order to calculate the auto power spectral density function (APSD) of a given time series, the time series are first resampled to arrive at an equidistant data set. Here, sample & hold is used. In single phase this is known to distort the high-frequency end of the APSD (see e.g. Adrian & Yao 1987). However, it was reported in (Mudde *et al.* 1997*a*) that in bubbly flow no difference was seen between sample & hold and linear interpolation. Once the data set is made equidistant, the APSD is calculated using FFT-based routines. To increase the accuracy of the estimate of the APSD, the data set is cut into records (that have an overlap of 50%). For each record, the mean is subtracted and the data are windowed using a Hanning window. Furthermore, zero-padding is applied. Finally, the APSDs of all records are averaged. The relative

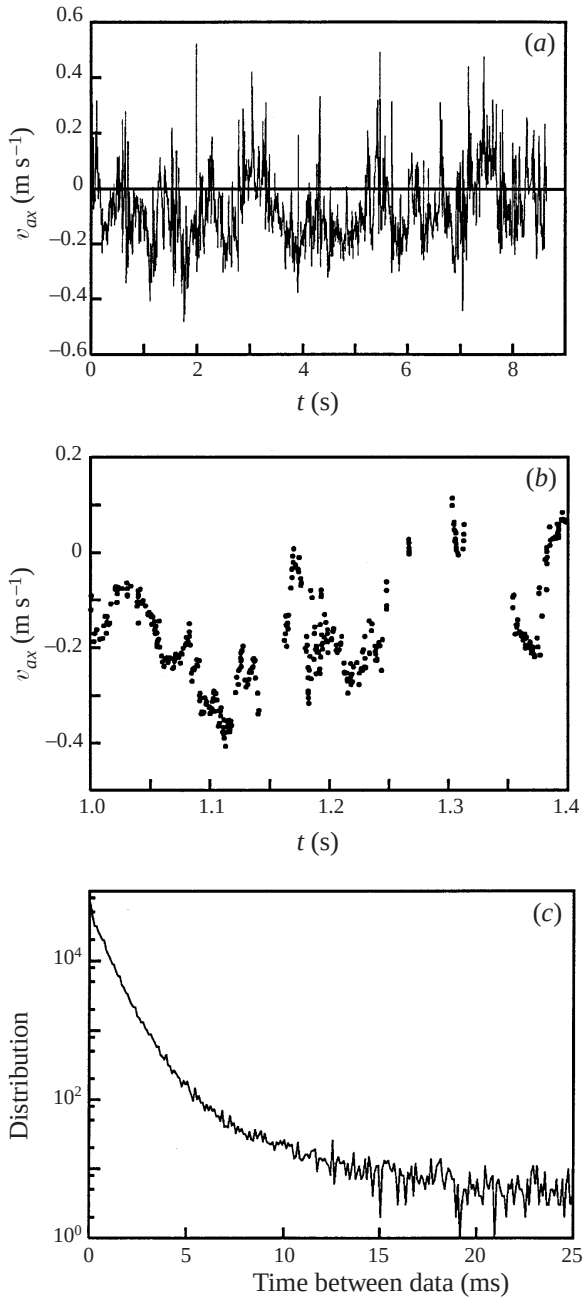

FIGURE 9. (*a*) Part of time series of the axial liquid velocity at $r/R = -0.88$ (bubble column mode); (*b*) zoom in on short time scales; (*c*) corresponding time between data distribution of entire time series.

inaccuracy of the estimated averaged APSD is proportional to the inverse of the square root of the number of records used. Note, that the length of the records cannot be chosen arbitrarily small, but should be sufficient to capture all relevant time scales present in the data sets.

4. Results

4.1. *Description of experiments*

Two experiments were performed:

(i) Bubble column mode: the pipe is filled with water up to an ungassed height of 618 cm above the gas sparger. The gas flow rate is set at 20 l min^{-1}, i.e. a superficial gas velocity of 1.83 cm s^{-1} (both evaluated at a pressure of 1 bar). The volume-averaged gas fraction, based on the increase of the mixture level, is 5.18%.

(ii) Bubbly pipe flow mode: the pipe is completely filled with liquid. The pump is set at a superficial liquid velocity of 0.175 m s^{-1} (i.e. Reynolds number based on superficial liquid velocity and water properties is 2.6×10^4), pumping the water vertically, upward through the pipe. The gas flow rate is 40 l min^{-1} (also evaluated at 1 bar).

The latter was chosen such that the averaged void fraction is close to that from the bubble column experiments.

All experimental data are taken at a height of 470 cm above the gas distributor.

The bubbly pipe flow is driven by both the bubbles and the pressure applied by the pump; the bubble column, obviously, only by the bubbles. In both cases two driving forces exist: (i) the average total pressure gradient ($\nabla p_t \equiv \nabla p + \rho_{liq} g$), and (ii) the average bubble driving force ($F_b \equiv \rho_{liq} g \langle \alpha \rangle$). An estimate of the relative importance of the two driving mechanisms can be made on the basis of a force balance. In the well-developed region of the flow, the wall shear stress τ_w, exerted by the fluid on the wall, balances the averaged pressure gradient as well as the force induced by the bubbles

$$\tau_w = \frac{D}{4} (F_b - \nabla p_t) \tag{9}$$

with $\langle \alpha \rangle$ the cross-sectional-averaged gas fraction, D the pipe diameter and ρ_{liq} the density of the liquid phase. The characteristics of the flow depend on the value of the two driving forces. For the bubble column the liquid flow close to the wall is downwards. The velocity at the wall is, obviously, zero. The thickness of the wall layer is on the order of 1 mm, whereas the downward velocity, u_d, is of the order of 15 cm s^{-1} (see below). Hence, the magnitude of the wall shear stress is estimated as $\eta u_d / \delta = 0.15$ Pa. The corresponding 'bubble stress', $(D/4)F_b$ is for the present experiments on the order of 15 Pa. So, clearly the two driving forces balance one another: $F_b \approx \nabla p_t$. Note that the pressure gradient in the bubble column mode is a reaction by the system to the applied bubble driving force and is not due to the action of a pump. In the present experiment for the bubbly pipe flow case, τ_w is positive and its value is estimated using the superficial liquid velocity and the Fanning friction factor for single-phase flows:

$$\tau_w = f \tfrac{1}{2} \rho_{liq} \left(U_{sup}^{liq} \right)^2 = 0.1 \text{ Pa} \tag{10}$$

where f denotes the Fanning friction factor.

Thus, for the bubbly pipe flow, the ratio of the two driving forces can be estimated as

$$\frac{F_b}{\nabla p_t} \approx 0.99. \tag{11}$$

Similarly, for the bubble column one finds $F_b / \nabla p_t \approx 1.01$. Consequently, a great similarity between the two modes is expected. Obviously, this similarity breaks down close to the wall as the mean axial liquid velocity close to the wall has a rather high negative value in the bubble column mode and is close to zero in the bubbly pipe

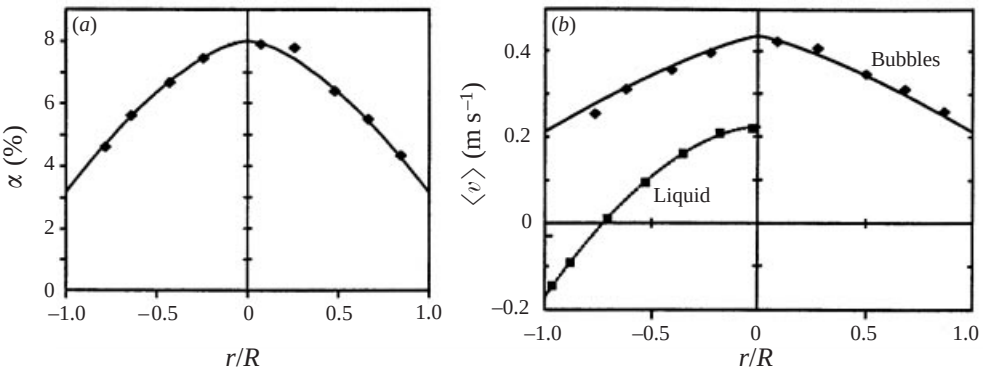

FIGURE 10. Bubble column, radial profile of: (*a*) the gas fraction and (*b*) the time-averaged axial component of the liquid velocity (■) and bubbles (◆).

flow mode. Nevertheless, as this difference is expected to be present in a thin layer close to the wall, the bulk of the flow is expected to show great similarities in both bubble modes.

4.2. *Bubble column*

A radial scan of the gas fraction, measured with the optical probe, is presented in figure 10(*a*). The solid line represents a fit (in the least-squares sense) of the form

$$\alpha(r/R) = \alpha_0 \left(1 - c \left(\frac{r}{R}\right)^p\right). \tag{12}$$

It is clear from the plot, that the gas fraction is symmetric; the average gas fraction, assuming cylinder symmetry, is $\langle\alpha\rangle = 5.27\%$ (the fit coefficients are $\alpha_0 = 8.0\%$, $c = 0.605$ and $p = 1.547$). This value is in good agreement with the volume-averaged gas fraction mentioned above. Comparing the value of p found with other data on the gas fraction distribution in bubble columns shows that the present profile is relatively steep. Usually a value of p around 4 or higher is reported for gas fractions of about 5% (see e.g. Kumar *et al.* 1994). This might be a consequence of the much higher height-to-diameter ratio that is used in the present experiments. Usually in bubble columns, a ratio of 8–10 is used. Here we have a ratio of 44 and we measure at a height corresponding to a ratio of 31.5. Hills (1974) reported differences in the steepness of the radial gas fraction distribution when using different perforated plates. Hence, the sparger used here might also be partly responsible for the relatively low value of p.

The radial profile of the time-averaged axial liquid velocity, measured at the same height, is given in figure 10(*b*). The familiar large-scale circulation is found. A fit of the form

$$\langle v\rangle(r/R) = (v_0 - v_w)\left(1 - \left(\frac{r}{R}\right)^m\right) + v_w \tag{13}$$

is also drawn ($v_0 = 0.223\,\mathrm{m\,s^{-1}}$, $v_w = -0.173\,\mathrm{m\,s^{-1}}$, $m = 1.780$). The profile crosses the axis at $r/R = 0.72$. Combining the fitted profile of the gas fraction and the liquid velocity gives a net liquid flow, $\pi R^2\langle(1-\alpha)v\rangle$, of $1.51\,\mathrm{s^{-1}}$, which is only 3% of the upward liquid flow (i.e. for $r/R < 0.72$), showing the accuracy of the measurements of the liquid velocity.

Also in figure 10(*b*) the averaged vertical velocity of the bubbles is given. The bubble velocity is measured using the four-point probe as described in § 4.1. It is

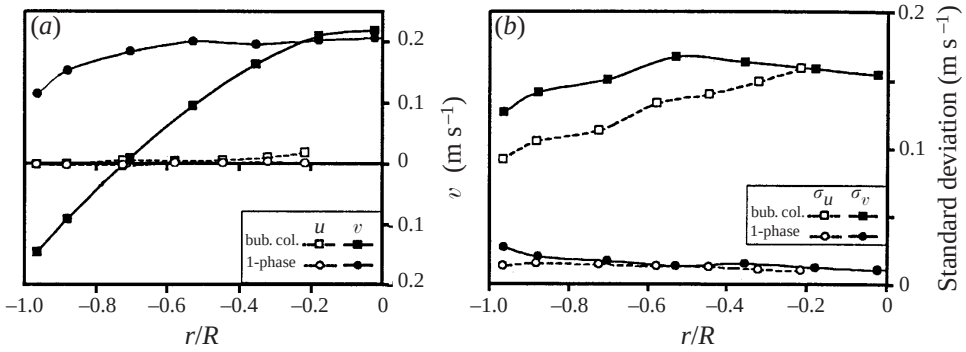

FIGURE 11. Radial profiles: (*a*) the mean liquid velocity for single-phase flow (1 phase: $U_{sup}^{liq} = 0.175\,\mathrm{m\,s^{-1}}$, $Re = 2.6 \times 10^4$) and bubble column (bub col: $U_{sup}^{gas} = 1.83\,\mathrm{cm\,s^{-1}}$). Open symbols: tangential velocity, u, closed symbols: axial velocity, v, and (*b*) standard deviation of mean liquid velocity (same key as in (*a*)).

important to realise that the probe is inserted with the tips facing downward. Thus, only the vertical rise velocity of the bubbles can be measured. Consequently, in the wall region the mean bubble velocity is biased towards higher positive values. This seems to be clear from the plot: the difference between the average bubble velocity and the mean liquid velocity increases with increasing radial position. The slip velocity at the centre of the column is $0.22\,\mathrm{m\,s^{-1}}$. This is in good agreement with the expected slip velocity based on the terminal velocity of a single bubble ($0.25\,\mathrm{m\,s^{-1}}$ for bubbles of the present size) and the local gas fraction in the column centre (about 8%). Applying Richardson & Zaki's relation for the slip velocity in a swarm gives for these numbers $0.22\,\mathrm{m\,s^{-1}}$. In the wall region the liquid flow is on average downwards: the mean velocity is approximately $-0.17\,\mathrm{m\,s^{-1}}$. This would imply a bubble velocity of about $0.05\,\mathrm{m\,s^{-1}}$. Obviously, a picture based on the (time-) averaged behaviour of the two-phase flow is inadequate to explain the observed phenomena. This will be discussed in more detail below.

From a fit of the radial profile of the mean bubble velocity and the fit of the radial gas fraction profile given above, the total gas flow is estimated. The result is $18.1\,\mathrm{l\,min^{-1}}$. At the experimental station the gas flow rate is $17\,\mathrm{l\,min^{-1}}$. Thus the measured gas flow rate is close to the applied gas. This seems to suggest that the mean bubble velocity is reasonably well estimated from the probe measurements.

It is well known (Chen *et al.* 1994; Lin *et al.* 1996; Yang *et al.* 1993; Devanathan *et al.* 1990; Devanathan, Moslemian & Dudukovi\'c 1995, Groen *et al.* 1995, 1996; Mudde *et al.* 1997*a*) that the precise behaviour of a bubble column can only be understood if large-scale structures present in the flow are taken into account. These structures also play an essential role here. Their presence has been found in the APSD of e.g. the vertical component of the liquid velocity (see e.g. Mudde *et al.* 1997*a*). They are also reflected in the large value of its standard deviation: the standard deviation of the axial component of the liquid velocity has a rather flat radial profile with a value of about $0.15\,\mathrm{m\,s^{-1}}$. This is an order of magnitude higher than for single-phase flow. For instance, the standard deviation of the axial component for water flow only at a mean velocity of $0.175\,\mathrm{m\,s^{-1}}$ varies from $0.01\,\mathrm{m\,s^{-1}}$ in the centre of the pipe to $0.027\,\mathrm{m\,s^{-1}}$ close to the wall. The radial profiles of the averaged liquid velocity and the corresponding standard deviation are plotted in figure 11.

The standard deviations (i.e. the normal stresses) of single-phase flow for the

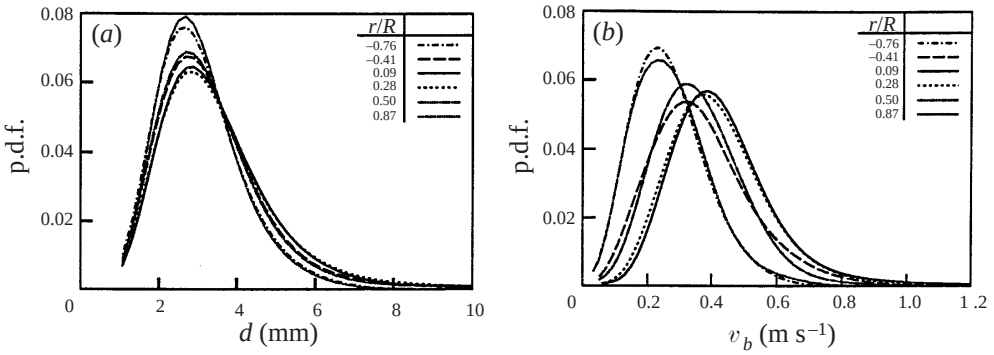

FIGURE 12. Probability density function of (*a*) bubble size and (*b*) vertical upward bubble velocity at various positions (bub. col.: $U_{sup}^{gas} = 1.83\,\mathrm{cm\,s^{-1}}$).

tangential and vertical component differ slightly (the difference should be a factor of 1.2). Furthermore, the normal stresses increase slightly towards the wall (see e.g. Townsend 1956 for a detailed discussion). However, in case of two-phase flow this is no longer the case. The vertical component of the normal stress is substantially larger than that of the tangential one. Furthermore, the radial profiles of both stresses in the two-phase flow show a clear increase with decreasing radial coordinate.

With the four-point probe at each radial position 10 measurement series were taken, each of 40 s with a sampling frequency of 20 kHz for each tip. In each series 150 to 450 bubbles hit the probe (depending on the radial position, obviously more hits in the centre than close to the wall). About 1/3 of these were validated for velocity measurement, using the criteria mentioned in § 3. Hence, at each radial position at least 500 valid bubbles were analysed. The data collected with the four-point probe show that the bubble size distribution is rather narrow. The vertical diameter of the bubbles has a mean value of 2.5 to 3.0 mm for almost all radial positions. In the centre of the column, the bubble size distribution is somewhat wider than close to the wall (see figure 12). The number of large bubbles (with a size of about 1 cm or larger) is very small; these bubbles can not be responsible for the large scale circulation or the vortical structures observed in the flow. The bubble velocity distribution is also given in figure 12. As expected, the bubbles close to the centre move faster than those close to the wall. Nevertheless, even in the centre bubbles with rather low velocity are detected. Again, the time-dependent nature of the flow is seen here. Note again, that the p.d.f.s for a position close to the wall are biased more than those for the centre: no negative velocities can be detected. This could explain why the p.d.f.s for the centre are wider than those close to the wall.

4.3. *Bubbly pipe flow*

Experiments are performed at a superficial liquid velocity of $0.175\,\mathrm{m\,s^{-1}}$, i.e. a Reynolds number of 2.6×10^4 (based on the pipe diameter, the superficial liquid velocity and the properties of water). The superficial gas velocity is set at $U_{sup}^{gas} = 3.66\,\mathrm{cm\,s^{-1}}$ giving an averaged gas fraction of 5.53%. A plot of the radial distribution of the averaged gas fraction is given in figure 13(*a*). In this figure the gas fraction data of the bubble column are also plotted.

It is amazing to see how closely the two profiles match. In bubbly flow in pipes of small diameter researchers (Serizawa, Kataoka & Michiyoshi 1975; Wang *et al.* 1987) have reported flat gas fraction profiles with wall peaking. However, investigation of

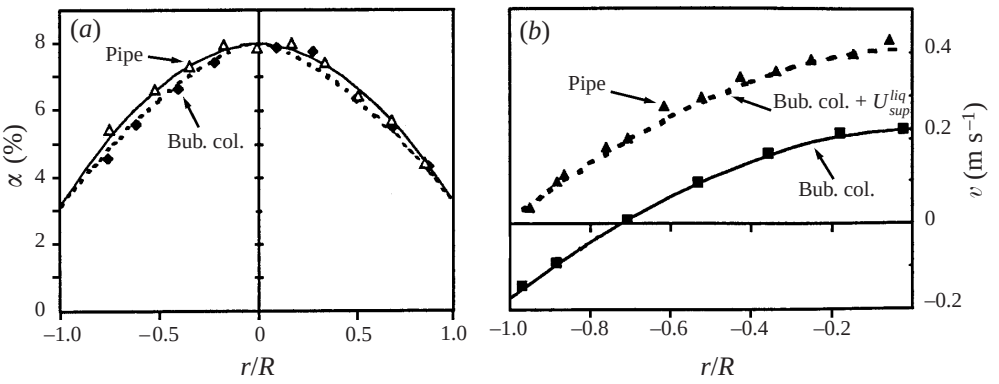

FIGURE 13. (*a*) Radial profile of the gas fraction (pipe flow: △, bub. col.: ◆) and (*b*) of time-averaged axial component of the liquid velocity, (pipe flow ▲: $U_{sup}^{liq} = 0.175\,\mathrm{m\,s^{-1}}$ ($Re = 2.6 \times 10^4$), $U_{sup}^{gas} = 3.66\,\mathrm{cm\,s^{-1}}$; bub. col.: ■).

air lift reactors (an excellent example is Young *et al.* 1991) revealed no wall peaking and a maximum gas fraction at the axis of the column. The gas fraction profile reported by Young *et al.* (1991) is, however, in most cases flatter than ours and not as symmetric. The value of $p = 1.547$ is surprisingly close to the one mentioned by Young *et al.* (1991) who found a value of 1.57 for a riser of 19 cm inner diameter (and a downcomer of 14 cm) at a superficial gas velocity of $2.1\,\mathrm{cm\,s^{-1}}$. For a superficial gas velocity of $4.7\,\mathrm{cm\,s^{-1}}$ Young *et al.* (1991) found a value of 1.75.

The radial profile of the time-averaged axial liquid velocity is given in figure 13(*b*). Here the similarity with the same profile for the bubble column mode is even more striking. The solid line represents the axial velocity in the bubble column mode. The dashed line is the axial velocity in the bubble column mode plus the superficial liquid velocity induced by the pump (i.e. $0.175\,\mathrm{m\,s^{-1}}$). This dashed line is a very good representation of the axial velocity profile in case of the bubbly pipe flow. In other words, the axial liquid velocity in the bubbly pipe flow case is a superposition of the superficial liquid velocity and the large-scale circulation that is so characteristic for the bubble column. To the best of our knowledge, this has never been reported in the literature.

The value of the exponent $m = 1.78$ (for the liquid velocity profile, see (13)) in our case is again in excellent agreement with the data of Young *et al.* (1991)) being 1.64 (superficial gas velocity $2.1\,\mathrm{cm\,s^{-1}}$) and 1.83 (superficial gas velocity $4.7\,\mathrm{cm\,s^{-1}}$). An estimate of the liquid superficial velocity from the radial gas fraction profile and the measured averaged liquid velocity profile gives a value of $0.19\,\mathrm{m\,s^{-1}}$, again in good agreement with the imposed value.

Finally, the radial bubble velocity distribution is given in figure 14. Here, the data of the bubble velocity for the bubble column have been shifted by the mean liquid velocity of the bubbly pipe flow. Again the data collapse on a single line. This is a surprise since in the bubble column mode the bubble velocities close to the wall are biased towards positive velocities as the probe cannot measure negative bubble velocities. However, in the pipe flow mode, the majority of bubble velocities expected is still positive and the biasing should be less. On the other hand the number of bubbles arriving at the probe in a given time interval depends on the bubble velocity in that interval. In this way the biasing is also present in the pipe flow mode (similar velocity biasing is known in LDA measurements). The difference cannot be attributed

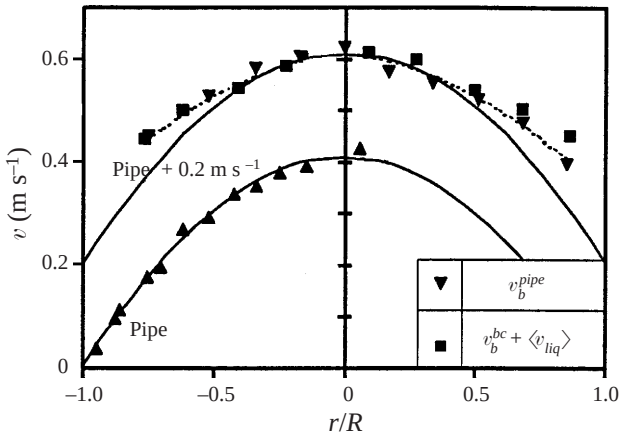

FIGURE 14. Pipe flow: radial profile of the time-averaged axial component of the liquid velocity (▲) and the bubble velocity (▼). Also the bubble velocity data for the bubble column (■) offset by the cross-sectional-averaged liquid velocity of the pipe flow are plotted. The full lines are a fit of the liquid velocity and of the liquid velocity offset by 0.2 m s^{-1}. The dashed line is a fit through the bubble velocity data of the pipe flow.

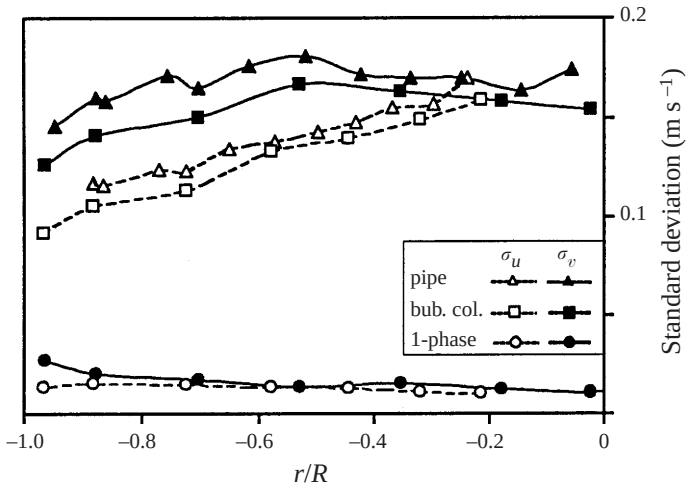

FIGURE 15. Radial profiles: standard deviation of the mean liquid velocity for single-phase flow (1 phase: $U_{sup}^{liq} = 0.175\,\mathrm{m\,s^{-1}}$), bubble column (bub. col.: $U_{sup}^{gas} = 1.83\,\mathrm{cm\,s^{-1}}$)) and pipe flow (pipe: $U_{sup}^{liq} = 0.175\,\mathrm{m\,s^{-1}}$, $U_{sup}^{gas} = 3.66\,\mathrm{cm\,s^{-1}}$). Open symbols: tangential velocity, u, closed symbols: axial velocity, v.

to a difference in slip velocity due to radial gas fraction as the variation is too small in the latter. Whether it is completely due to 'velocity-bias' cannot be determined from the present experiments. If the gas flow rate is estimated from the experimental gas fraction and the bubble velocity profile a value of 29.31 min^{-1} is found, whereas the actual value at the experimental position is 301 min^{-1}. Again the agreement is good.

The standard deviation for the tangential and axial component of the liquid velocity is given in figure 15. Again a great similarity between the bubble column mode and the bubbly pipe flow is observed. In both cases the standard deviation of the axial velocity component is significantly higher than that of the tangential component.

Even more striking is that, also for the standard deviation, the value for bubbly pipe flow is close to the sum of the single-phase standard deviation and the bubble column one. This suggest a superposition of the 'turbulence' as well. Apparently, the action of gravity on non-uniformities in the bubble distribution is similar in both bubble cases. To find whether or not this is universal needs much more research, with different gas fractions and different pipe diameters. Nevertheless, the results obtained here seem to suggest that the structures reported in research on bubble columns are also present in the case of bubbly pipe flow. This could then very well be generalized to air lift loops.

Lance & Bataille (1991) investigated the influence of bubbles on the turbulence in grid-generated turbulent flow in a rectangular pipe (45 cm × 45 cm in cross-section). They reported a strong increase in the turbulence beyond a critical gas fraction of about 1.2% in their experiment. This was connected to a critical bubble–bubble distance beyond which bubble–bubble interaction becomes important. If the extra turbulent energy compared to single phase flow only is attributed to 'local stirring' by the bubbles, two contributions can be identified: the (potential) flow of the liquid around a bubble and the wakes. The former would give a contribution to the standard deviation in the streamwise direction of

$$\sqrt{\tfrac{1}{5}\alpha}U_{slip} \tag{14}$$

which is roughly equal to $0.03\,\mathrm{m\,s^{-1}}$. The latter can be estimated from the dissipation rate due to the work performed by the drag force. Assuming that the associated length scale for the dissipation is of the order of the bubble diameter, the contribution of this effect to the standard deviation is (see e.g. Lance & Bataille 1991),

$$(\alpha C_D)^{1/3}U_{slip} \tag{15}$$

i.e. about $0.09\,\mathrm{m\,s^{-1}}$ (with C_D the drag coefficient).

The fluctuations of e.g. the axial component of the liquid velocity can be thought of as being a combination of effects: (1) (single-phase) shear, (2) potential flow around the bubbles, (3) wakes, (4) other, like vortical, structures caused by non-uniform distribution of the bubbles. Formally, this can be written as

$$v'_{ax}\{t_j\} = v'_{ax,1}\{t_j\} + v'_{ax,2}\{t_j\} + v'_{ax,3}\{t_j\} + v'_{ax,4}\{t_j\}, \tag{16}$$

the standard deviation is then

$$\sigma = \left[\frac{1}{N}\sum_{i=1}^{N}\left(v'_{ax,1}\{t_j\} + v'_{ax,2}\{t_j\} + v'_{ax,3}\{t_j\} + v'_{ax,4}\{t_j\}\right)^2\right]^{1/2}. \tag{17}$$

Two extremes can easily be calculated:

(*a*) the various contributions are completely uncorrelated, i.e.

$$\frac{1}{N}\sum_{i=1}^{N}\left(v'_{ax,k}v'_{ax,l}\right) = \sigma_k^2\delta_{kl} \tag{18}$$

and thus for the standard deviation one finds

$$\sigma^2 = \sigma_1^2 + \sigma_2^2 + \sigma_3^2 + \sigma_4^2 \tag{19}$$

with σ_k the standard deviation of the fluctuating part $v'_{ax,k}$;

(*b*) the various contributions are completely correlated for all frequencies without

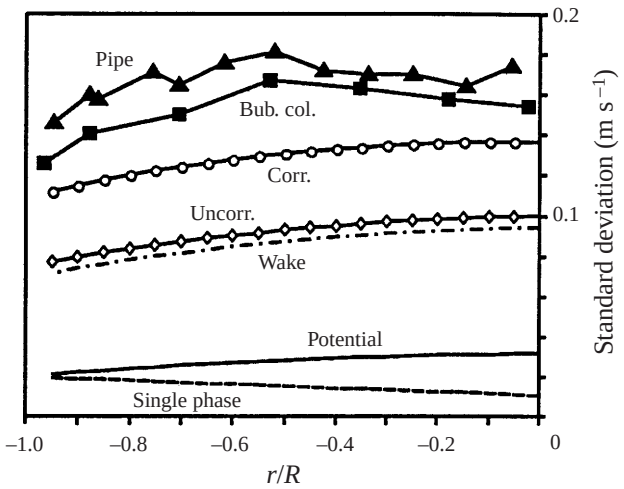

FIGURE 16. Comparison of the contribution of various phenomena to the standard deviation of the axial velocity.

phase-shift, i.e.

$$\frac{1}{N}\sum_{i=1}^{N}\left(v'_{ax,k}v'_{ax,l}\right) = \sigma_k\sigma_l \tag{20}$$

and one finds

$$\sigma^2 = (\sigma_1 + \sigma_2 + \sigma_3 + \sigma_4)^2 . \tag{21}$$

Obviously, case (*a*) underestimates the standard deviation as at least the two parts from the local stirring by the bubbles will probably show positive correlation. Case (*b*) on the other hand is an overestimation as it is very unlikely that the correlation is complete over all frequencies and shows no phase-shift. In figure 16 estimates for the first three contributions in equation (17) are given.

In the figure, the single-phase contribution from the single-phase experiments is given together with the estimates of the local bubble stirring (i.e. the potential flow and the drag/wake contributions). For the latter two, the estimates given above are used, taking the radial profile of the gas fraction into account. Furthermore, the total contribution of these three effects is given for the uncorrelated ($\diamond$) as well as the completely correlated ($\circ$) estimate. As can be seen from figure 16 these two extremes are insufficient to account for the high value of the standard deviation. Most likely, the contribution of the vortical structures is also of great importance in the bubbly pipe flow case.

With the optical probe at each radial position 20 series of measurements were taken at a frequency of 40 kHz. Each series has a length of 20 s. The number of bubbles in a series hitting the probe ranges again from 150 close to the wall to 450 in the centre. Also here roughly 1/3 is validated, hence a minimum of 1000 pieces of velocity and size data per radial position are obtained. The probability density functions of the bubble diameter and bubble rise velocity for the pipe flow case are given in figure 17. The distribution of the bubble diameters for the pipe flow is quite comparable to that for the bubble column (see figure 12). Also the distribution of the bubble velocities is comparable in the two cases, although, obviously, the pipe flow p.d.f.s are shifted to higher velocities by roughly the superficial liquid velocity. Note further,

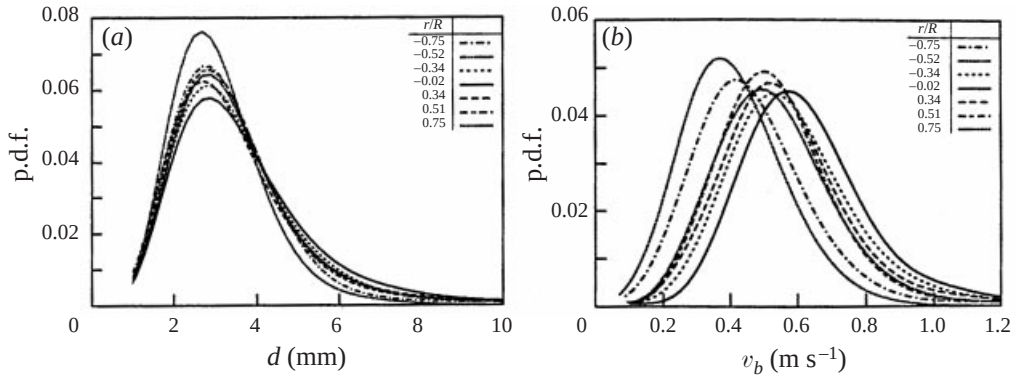

FIGURE 17. Probability density function of bubble size (*a*) and vertical upward bubble velocity (*b*) at various positions ($U_{liq} = 0.175\,\mathrm{m\,s^{-1}}$, $\phi_{gas} = 0.401\,\mathrm{min^{-1}}$).

that the velocity p.d.f.s for the pipe flow are wider than the corresponding ones for the bubble column. This has probably two reasons. First, already mentioned above, the optical fibre probe cannot measure 'negative' velocities. Hence, the results for low bubble velocities are biased towards the higher ones. This makes the velocity-p.d.f.s for the bubble column measured at positions close to the wall more narrow than they are in reality. This is clear in figure 12(*b*): the velocity-p.d.f.s at $r/R = -0.76$ and 0.87 are both significantly narrower than the others. In the case of pipe flow (figure 17*b*) this is not the case; here all p.d.f.s have about the same width. Second, the standard deviation of the liquid velocity in the pipe flow is some 10% higher than for the bubble column. Since the local liquid velocity and the bubble velocity are coupled (their difference is the slip velocity that is almost constant) it seems reasonable to expect that the velocity-p.d.f. of the bubbles is wider in the case of pipe flow than that of the bubble column. It is seen in figures 17(*b*) and 12(*b*) that indeed the velocity-p.d.f.s for the pipe flow are about 10% wider than the corresponding ones for the bubble column. The above again points to the similarity of the pipe flow and the flow in the bubble column.

4.4. *Power spectrum*

The time series of the axial component of the liquid velocity at $r/R = -0.88$ are used to further compare the two bubbly flow modes. The data set of the axial velocity for the bubbly pipe flow is taken as reference. This set has a length of 999.4 s, containing 426 755 velocity points. First, this set is made equidistant by resampling with a sample time corresponding to the mean data rate, i.e. 2.342 ms. Second, the set is divided into 51 records of 16 384 data points (corresponding to a time interval of 38.37 s). Finally the APSD of each record is calculated and the average APSD is obtained. The same is done using the time series of the axial component of the velocity at the same location, but now measured in the bubble column mode. This series is also resampled with 2.342 ms. The average APSD is calculated using records of the same length (16384 points, 38.37 s). As the mean data rate of this series was higher and the total length of the series shorter, the number of records used is 16. The two APSDs are compared in figure 18. It is clear from the figure that the frequency content of the two series is almost the same. The total power of the data set for the bubbly pipe flow mode is slightly higher. This is in agreement with the somewhat higher standard deviation of the liquid velocity in the pipe flow mode, as the power and standard

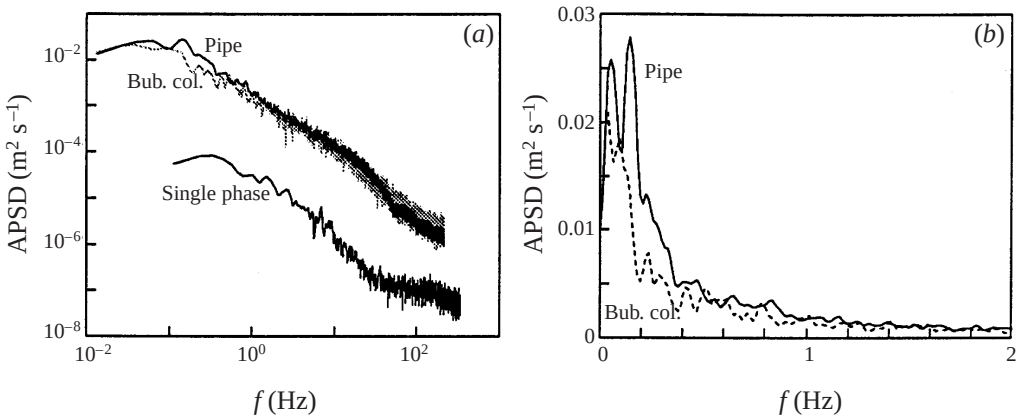

FIGURE 18. (*a*) Auto power spectral density function of vertical liquid velocity at $r/R = -0.88$; (*b*) zoom in on low-frequency part for bubble column and bubbly pipe flow.

deviation are linked through Parseval's identity:

$$\int |V(f)|^2 \mathrm{d}f = \int |v(t)|^2 \mathrm{d}t \tag{22}$$

with $V(f)$ the Fourier transform of $v(t)$. Note that also in figure 18 the APSD of the axial liquid velocity time series for single-phase flow at $r/R = -0.88$ is given. The APSD is two orders of magnitude lower than the APSDs for the bubbly flow, again in good agreement with the standard deviation that is an order of magnitude lower for the single-phase flow.

As the two spectra for the bubbly flows are almost identical, it is no surprise that the integral time scale of both will be about the same. This time scale is estimated as

$$\mathscr{T} = \int_0^\infty ACF(t)\mathrm{d}t \tag{23}$$

where $ACF(t)$ denotes the auto-correlation function of the liquid velocity time series. For both bubbly flows, the integral time scale is about 0.45 s.

In figure 18(*b*) a zoom-in on the low-frequency content of the APSDs for the bubbly flow is given (on a linear scale). Both show a significant peaking at low frequencies. This is attributed to the occurrence of vortical structures in the flow. In bubble columns these have been reported by e.g. Chen *et al.* (1994) and Mudde *et al.* (1997*a*). Here it is found that they are also present in the bubbly pipe flow mode, at similar frequencies as in the bubble columns.

4.4.1. *Short-time frequency analysis*

In the above spectra, no information is available on the occurrence of the vortical structures in time. Mudde *et al.* (1997*a*) used short-time frequency analysis to study the evolution in time of the low-frequency content of the liquid velocity time series. To this end the velocity time series is time-windowed before the spectrum is calculated (see e.g. Qian & Chen 1996). For the time-window a box window, $\gamma(t)$, is used:

$$\gamma(t) = \begin{cases} 1 & \text{if } T \leqslant t \leqslant T + \Delta T \\ 0 & \text{otherwise.} \end{cases} \tag{24}$$

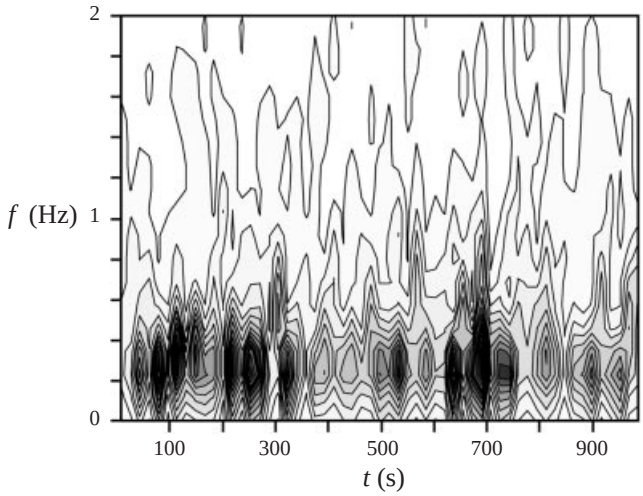

FIGURE 19. Contour plot of the time-dependent spectrum of the axial velocity at $r/R = -0.76$ (bubbly pipe flow).

The corresponding spectrum is then obtained from

$$APSD(T,f) = |STFT(T,f)|^2 \tag{25}$$

with

$$STFT(T,f) = \int v(t)\gamma(t)\mathrm{e}^{2\pi i f t}\mathrm{d}t. \tag{26}$$

By sliding the time-window over the time series, the evolution of the frequency content of the velocity time series in time is estimated. In figure 19 the time-dependent power spectrum of the axial liquid velocity measured at $r/R = -0.76$ in the pipe flow mode is shown. For the high-frequency part of the spectrum, no significant changes with respect to the APSD of figure 18(*a*) are found. However, the low-frequency part in figure 19 clearly shows the 'eruption' of low-frequency fluctuations. These are most likely the vortical structures that pass the measuring point. The figure consists of 57 spectra, with a time-separation of 17.45 s. The frequency resolution is 0.115 Hz. As is clear from the plot, the arrival of these structures is irregular in time; they are not present all the time, i.e. some 14 (out of a possible 57) 'eruptions' are seen. Obviously, no hard conclusions can be drawn from this plot as the time chosen between two consecutive spectra acts as a filter on the resolution of the structures. Wavelet analysis will be more appropriate for studying the occurrence of them. However, changing the length of the window function by a factor of two (or half) does not change the time-frequency plot significantly with respect to the 'eruptions': they appear at about the same time (and hence in the same number).

Analysis of other time series, either from the bubbly pipe flow or bubble column mode, shows similar spectra.

5. Concluding remarks

The local hydrodynamics of a bubbly flow in a 0.149 m inner diameter vertical pipe have been investigated. For the gas fraction, bubble rise velocity and bubble diameter a four-point optical fibre probe has been used. LDA was applied to study the liquid flow field. Two operation modes have been used: the bubble column and bubbly pipe

flow. For both cases the averaged gas fraction was set at about 5.4%. For the bubbly pipe flow, the liquid was pumped upwards through the pipe at a superficial velocity of $0.175\,\mathrm{m\,s^{-1}}$.

The most striking finding in the experiments is the great similarity between the two experiments. This holds not only for the qualitative results, but even quantitatively the two are very similar. The radial gas fraction distribution and that of the mean vertical liquid and bubble velocities are identical for both operation modes except for an offset of the velocity profiles, of course. This offset is close to the superficial liquid velocity. The similarity between the two bubbly flows was expected from a simple analysis of the relative importance of the driving forces due to the pressure gradient on the one hand and to the bubbles on the other hand. This analysis showed that in both cases the two driving forces are of almost the same magnitude. Furthermore, since the averaged gas fraction in the two modes is the same, the forces in both cases are almost identical. The similarity holds not only for the mean velocities and gas fraction, but also for the turbulence. The turbulence intensities in both modes, represented by the standard deviation in the liquid velocity, are comparable in magnitude and much higher than for the corresponding flow rate in single phase only. The intensity in the bubbly pipe flow mode is found to be somewhat higher than in the bubble column mode. The difference between the two is of the same order of magnitude as the turbulence intensity in the single phase flow. The standard deviation of the tangential liquid velocity component is lower than that of the axial one. The power spectral density functions of the fluctuating part of the liquid velocity for bubbly flows are found to be almost identical at all frequencies. Both in the bubbly pipe flow and the bubble column mode, vortical structures, that manifest themselves as low-frequency 'eruptions' in the spectra, are found.

The bulk of the bubbly pipe flow is in essence equivalent to the flow of the bulk in a bubble column, but 'slowly' being displaced upwards. Of course, close to the wall differences should be present. The picture that seems to emerge from the experiments is that the bubbly pipe flow is a superposition of the single-phase flow at the same liquid flow rate and the bubble column at the same gas fraction. Similar experiments with a higher accuracy are needed for a more general evidence. If this turns out to be a general feature of bubbly pipe flow, a unification between the description of the hydrodynamics of a bubble column and that of an air lift should be possible.

The authors would like to thank Dr Luis Portela and Dr Jos Derksen for stimulating discussions.

REFERENCES

Adrian, R. J. & Yao, C. S. 1987 Power spectra of fluid velocities measured by laser Doppler velocimetry. *Exps. Fluids* **5**, 17–28.

Bauer, M. & Eigenberger, G. 1999 A concept for multi-scale modeling of bubble columns and loop reactors. *Chem. Engng Sci.* **54**, 5109–5118.

Cartellier, A. 1992 Simultaneous void fraction measurement, bubble velocity, and size estimate using a single optical probe in gas-liquid two-phase flows. *Rev. Sci. Instrum.* **63**, 5442–5453.

Chen, R. C., Reese, J. & Fan, L.-S. 1994 Flow structure in a three-dimensional bubble column and three-phase fluidized bed. *AIChE J.* **49**, 1093–1104.

Chisti, M. Y., Halrd, B. & Moo-Young, M. 1988 Liquid circulation in airlift reactors. *Chem. Engng Sci.* **43**, 451–457.

Cockx, A., Do-Quang, Z., Liné, A. & Roustan, M. 1999 Use of computational fluid dynamics for simulating hydrodynamics and mass transfer in industrial ozonation towers. *Chem. Engng Sci.* **54**, 5085–5090.

Cockx, A., Liné, A., Roustan, M., Do-Quang, Z. & Lazarova, V. 1997 Numerical simulation and physical modeling of the hydrodynamics in an air-lift internal loop reactor. *Chem. Engng Sci.* **52**, 3787–3793.

Deckwer, W.-D. 1992 *Bubble Column Reactors.* Wiley.

Devanathan, N. 1991 Investigation of liquid hydrodynamics in bubble columns via a computer automated radioactive particle tracking (CARPT) facility. PhD thesis, Washington University in Saint Louis, Missouri, United States of America.

Devanathan, N., Duduković, M. P., Lapin, A. & Lübbert, A. 1995 Chaotic flow in bubble columns. *Chem. Engng Sci.* **50**, 2661–2667.

Devanathan, N., Moslemian, D. & Duduković, M. P. 1990 Flow mapping in bubble columns using CARPT. *Chem. Engng Sci.* **45**, 2285–2291.

Franz, K., Börner, T., Kantorek, H. J. & Buchholz, R. 1984 Flow structures in bubble columns. *Ger. Chem. Engng* **7**, 365–374.

Frijlink, J. J. 1987 Physical aspects of gassed suspension reactors. PhD thesis, Delft University of Technology, The Netherlands.

Geary, N. W. & Rice, R. G. 1992 Circulation and scale-up in bubble columns. *AIChE J.* **38**, 76–82.

Gharat, S. D. & Joshi, J. B. 1992 Transport phenomena in bubble column reactors 1: flow pattern. *Chem. Engng J.* **48**, 141–151.

Grevskott, S., Sannæs, B. H., Duduković, M. P., Hjarbo, K. W. & Svendsen, H. F. 1996 Liquid circulation, bubble size distributions, and solids movement in two- and three-phase bubble columns. *Chem. Engng Sci.* **51**, 1703–1714.

Groen, J. S., Mudde, R. F. & Van Den Akker, H. E. A. 1995 Time dependent behaviour of the flow in a bubble column. *Trans. Inst. Chem. Engrs* **74**, A 615–621.

Groen, J. S., Oldeman, R. G. C., Mudde, R. F. & Van Den Akker, H. E. A. 1996 Coherent structures and axial dispersion in bubble column reactors. *Chem. Engng Sci.* **51**, 2511–2520.

Hills, J. H. 1974 Radial non-uniformity of velocity and voidage in a bubble column. *Trans. Inst. Chem. Engrs* **52**, 1–9.

Kumar, S. B., Devanathan, N., Moslemian, D. & Duduković. M. P. 1994 Effect of scale-up on liquid circulation in bubble columns. *Chem. Engng Sci.* **49**, 5637–5652.

Lance, M. & Bataille, J. 1991 Turbulence in the liquid phase of a uniform bubbly air-water flow. *J. Fluid Mech.* **222**, 95–118.

Lin, T., Reese, J., Hong, T. & Fan L.-S.1996 Quantitative analysis and computation of two-dimensional bubble columns. *AIChE J.* **42**, 301–318.

Mercer, D. 1990 Flow characteristics of a pilot-scale airlift fermentor. *Biotech. & Bioengng* **29**, 988–994.

Mudde, R. F., Groen, J. S., Van Den Akker, H. E. A. 1997*a* Liquid velocity field in a bubble column: LDA experiments. *Chem. Engng Sci.* **52**, 4217–4224.

Mudde, R. F., Groen, J. S. & Van Den Akker, H. E. A. 1998 Application of LDA to bubbly flows. *Nucl. Engng Design* **184**, 329–338.

Mudde, R. F., Lee, D. J., Reese, J. & Fan, L.-S. 1997*b* The role of coherent structures on the Reynolds stresses in a two-dimensional bubble column. *AIChE J.* **43**, 913–926.

Mudde, R. F. & Van Den Akker, H. E. A. 1999 Dynamic behavior of the flow field of a bubble column at low to moderate gas fractions. *Chem. Engng Sci.* **54**, 4921–4927.

Ohnuki, A. & Akimoto, H. 2000 Experimental study on transition of flow pattern and phase distribution in upward air-water two-phase flow along a vertical pipe. *Intl J. Multiphase Flow* **26**, 367–386.

Qian, S. & Chen, D. 1996 *Joint Time-Frequency Analysis: Methods and Applications.* Prentice-Hall.

Sanyal, J., Vásquez, S., Roy, S. & Duduković, M. 1999 Numerical simulations of gas-liquid dynamics in cylindrical bubble column reactors. *Chem. Engng Sci.* **54**, 5071–5084.

Serizawa, A., Kataoka, I. & Michiyoshi, I. 1975 Turbulence structure of air-water bubbly flow-ii. local properties. *Intl J. Multiphase Flow* **2**, 235–246.

Townsend, A. 1956 *The Structure of Turbulent Shear Flow.* Cambridge University Press.

Ueyama, K. & Miyauchi, T. 1979 Properties of recirculating turbulent two phase flow in gas bubble columns. *AIChE J.* **25**, 258–266.

Wang, S., Lee, S., Jones, O. & Lahey, R. Jr 1987 Local void fraction measuring techniques in two-phase using hot-wire anemometry. *Intl J. Multiphase Flow* **23**, 327–343.

Yang, Y. B., Devanathan, N. & Duduković, M. P. 1993 Liquid backmixing in bubble columns via computer-automated radioactive particle tracking (CARPT). *Exps. Fluids* **16**, 1–9.

Young, M., Carbonell, R. & Ollis, D. 1991 Airlift bioreactors: analysis of local two-phase hydrodynamics. *AIChE J.* **37**, 403–428.